Nonmonotonic crossover in electronic phase separated manganite superlattices driven by the superlattice period

Yinyan Zhu,[1,2] Biying Ye,[1] Qiang Li,[1] Hao Liu,[1] Tian Miao,[1] Lijun Wu,[3] Lei Li,[4] Linfang Lin,[5] Yi Zhu,[1] Zhe Zhang,[6] Qian Shi,[1] Yulong Yang,[1] Kai Du,[1] Yu Bai,[1] Yang Yu,[1] Hangwen Guo,[1,2] Wenbin Wang,[1,2] Xiaoshan Xu,[7] Xiaoshan Wu,[6] Zhicheng Zhong,[4] Shuai Dong,[5] Yimei Zhu,[3] Elbio Dagotto,[8,*] Lifeng Yin,[1,2,9,†] and Jian Shen[1,2,9,‡]

[1]*State Key Laboratory of Surface Physics and Department of Physics, Fudan University, Shanghai 200433, China*
[2]*Institute for Nanoelectronics Devices and Quantum Computing, Fudan University, Shanghai 200433, China*
[3]*Condensed Matter Physics and Materials Science Department, Brookhaven National Laboratory, Upton, New York 11973, USA*
[4]*Key Laboratory of Magnetic Materials and Devices and Zhejiang Province Key Laboratory of Magnetic Materials and Application Technology, Ningbo Institute of Materials Technology and Engineering, Chinese Academy of Sciences, Ningbo 315201, China*
[5]*School of Physics, Southeast University, Nanjing 211189, China*
[6]*Department of Physics, Nanjing University, Nanjing 211189, China*
[7]*Department of Physics and Astronomy, University of Nebraska–Lincoln, Lincoln, Nebraska 68588, USA*
[8]*Department of Physics and Astronomy, University of Tennessee, Knoxville, Tennessee 37996, USA and Materials Science and Technology Division, Oak Ridge National Laboratory, Oak Ridge, Tennessee 37831, USA*
[9]*Collaborative Innovation Center of Advanced Microstructures, Nanjing University, Nanjing 210093, China and Shanghai Qi Zhi Institute, Shanghai 200232, China*

(Received 11 May 2020; revised 21 August 2020; accepted 12 November 2020; published 2 December 2020)

Studying manganite superlattices $[(LCMO)_{2n}/(PCMO)_n]_t$ made of $La_{0.625}Ca_{0.375}MnO_3$ (LCMO) and $Pr_{0.625}Ca_{0.375}MnO_3$ (PCMO), we found an unexpected behavior varying the period n. At small n, the ensemble is a three-dimensional ferromagnetic metal due to interfacial charge transfer. At large n, the LCMO layers dominate transport. However, rather than a smooth interpolation between these limits a sharp transport and magnetic anomaly is found at an intermediate critical PCMO thickness n^*. Magnetic force microscopy reveals that the phase-separation length scale also maximizes at n^* where, unexpectedly, it becomes comparable to that of the $(La_{1-y}Pr_y)_{0.625}Ca_{0.375}MnO_3$ (LPCMO) alloy. We conjecture the phenomenon originates in a disorder-related length scale: Large charge-ordered clusters as in LPCMO can only nucleate when Pr-rich regions reach a critical size related to n^*.

DOI: 10.1103/PhysRevB.102.235107

I. INTRODUCTION

The superlattice period often influences the global physical behavior of artificially engineered systems [1–4]. In the short period limit, superlattices are governed by interfaces, with emerging novel phenomena commonly observed [5–8]. In the long period, the superlattice behavior is dominated by individual components. In between these limits, the interlayer coupling between the interface layers determines the physical properties of the ensemble. Thus, the global physical properties with changing superlattice period are anticipated to reflect on the interplay between proximity effects, interlayer coupling, and the individual characteristics of the formation components. A smooth evolution is expected from one limit to the other. However, if experimentally determined physical properties of a superlattice exhibit instead a *nonmonotonic sharp* dependence on its period, then an unexpected characteristic length scale, not obvious "*a priori*," must be responsible for such unusual behavior.

For correlated oxide superlattices, besides the proximity effects and interlayer coupling [9–12], electronic phase separation (EPS) caused by competition of phases becomes important adding complexity into the system [13–18]. Here, we fabricate $La_{0.625}Ca_{0.375}MnO_3$ (LCMO) and $Pr_{0.625}Ca_{0.375}MnO_3$ (PCMO) superlattices with the form $[(LCMO)_{2n}/(PCMO)_n]_t$ to investigate the n dependence of the superlattice physical properties and EPS. The ground states of LCMO [19,20] and PCMO [21,22] are ferromagnetic metal (FM) and antiferromagnetic insulator (AFI), respectively. The LCMO and PCMO alloy, i.e., $(La_{1-y}Pr_y)_{0.625}Ca_{0.375}MnO_3$ (LPCMO), has a FM/AFI mixed-phase ground state where the EPS domain size is remarkably large, of submicron scale [23–26]. Surprisingly, in the $[(LCMO)_{2n}/(PCMO)_n]_t$ superlattice studied here, we observe a dramatic nonmonotonic n dependence of the FM-AFI phase transitions, with a sharp critical point at $n^* = 6$ or 7. Figure 1 contains a qualitative summary of the naively expected smooth interpolation, explaining that a broad peak in the resistivity should occur with varying n (see orange curve in Fig. 1) if only charge transfer at small n and individual component behavior at large n dominate.

*edagotto@utk.edu
†lifengyin@fudan.edu.cn
‡shenj5494@fudan.edu.cn

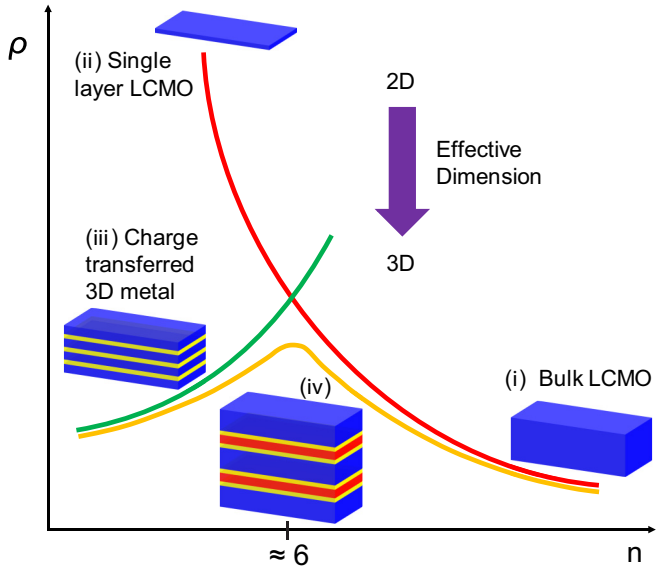

FIG. 1. Intuitive explanation of expected results in our superlattices. (i) Represents bulk metallic LCMO (blue) at large n, while (ii) represents just a LCMO single layer. The red curve is the idealized LCMO superlattice evolution (without PCMO) from 3D to 2D, i.e., from (i) to (ii). Naturally the resistivity increases by decreasing n; see text. Now consider our superlattice LCMO-PCMO. At small n, work function differences induce charge transfer from metal to insulator, panel (iii) (yellow is PCMO metallized by LCMO). Panel (iii) becomes, thus, metallic and 3D. Its resistivity is higher than 3D LCMO, because PCMO is insulatinglike even after charge transfer. Thus, $\rho(\text{iii}) > \rho(\text{i})$ as observed. As n grows from $n = 1$, the PCMO region affected by charge transfer covers a smaller fraction of PCMO (red); see panel (iv). Thus, $\rho(\text{iv}) > \rho(\text{iii})$, as observed, defining the green curve. Combining results, the orange curve emerges, naturally containing a broad peak. The big purple arrow indicates how the effective dimension changes in the figure. While this sketch contains the essence of our results, the observed intermediate peak is *much sharper* than here anticipated, revealing a conjectured length scale related to quenched disorder that renders the superlattice similar to the LPCMO alloy with giant phase separation.

However, instead of such a smooth evolution, here we found a far more subtle transition involving sharp peaks in several observables near n^*. Even more surprisingly, at n^* the Curie temperature (T_C), insulator to metal transition temperature (T_P), and even the EPS domain size are nearly identical to those of the LPCMO alloy, a totally unexpected result because a superlattice by construction should behave quite differently from a random alloy. We conjecture that this complex n-dependent behavior of the $[(\text{LCMO})_{2n}/(\text{PCMO})_n]_t$ superlattice is caused by the existence of a critical length scale related to the quenched disorder needed to nucleate the unusually large charge-ordered clusters typical of phase separated LPCMO. We emphasize that this disorder seed size (a few lattice spacings) is much smaller than the EPS cluster sizes in LPCMO (hundreds of lattice spacings) or in our superlattices at n^*: a disorder seed simply unbalances the competing effects between phases, in this case FM vs AFI states. This is analogous to a gentle push in a potential $V(x)$ when the particle is at a local maximum (unstable equilibrium). Essentially FM and AFI are in a fragile competition, and a small effect (in this case disorder) can totally tilt the balance in favor of one or the other.

II. RESULTS

We fabricate a series of $[(\text{LCMO})_{2n}/(\text{PCMO})_n]_t$ superlattices from $n = 1$ to 18. All the $[(\text{LCMO})_{2n}/(\text{PCMO})_n]_t$ superlattices are epitaxially grown on $SrTiO_3(100)$ substrates using laser molecular beam epitaxy (see "Sample preparation" in the Methods section of the Supplemental Material [27]). The superlattice's quality is monitored by *in situ* reflection high-energy electron diffraction (RHEED) intensity oscillations (Fig. S1 in the Supplemental Material [27]), and cross examined by *ex situ* x-ray diffraction (XRD) (Fig. S2 [27]) [28] and transmission electron microscopy (TEM) (Fig. S3 [27]). For comparison, LPCMO alloy thin films with the same total thickness and nominal chemical compositions are also epitaxially grown on $SrTiO_3$ substrates (Fig. S1(a) [27]). Magnetic and transport properties of the samples are respectively characterized using a superconducting quantum interference device (SQUID) and physical property measurement system (PPMS), and the EPS domain patterns are imaged by variable temperature magnetic force microscopy (MFM).

Figure S1(d) in the Supplemental Material [27] shows typical unit cell by unit cell RHEED intensity oscillations of a $[(\text{LCMO})_{10}/(\text{PCMO})_5]_{10}$ superlattice. There is distinguishable intensity difference between the LCMO (black) and the PCMO (red) layers. The superlattice period is cross examined by XRD measurements, where distinct superlattice peaks and fringe oscillations are seen (Fig. S2 [27]). Figure S3(a) [27] shows the high-angle annular dark field (HAADF) STEM image at $n = 5$. Although the contrast between LCMO and PCMO layers is not sharp, due to the small difference in atomic number between Pr and La, the HADDF image shows that the superlattice does not have noticeable defects or dislocations at the LCMO/PCMO interfaces. Figure S3(b) [27] contains the electronic energy loss spectrum (EELS) along the scan line (brown), clearly indicating well separated $M_{5,4}$ edges of La and Pr. The EELS image acquired from the marked box area (green) in Fig. S3(a) [27] is in Figs. S3(c) and S3(d) for La and Pr, respectively, with a color mixture shown in Fig. S3(e) [27]. The interfaces between LCMO and PCMO layers are atomically sharp without noticeable intermixing.

The transport and magnetic properties of the superlattices evolve nonmonotonically with increasing n. Figures 2(a) and S5 [27] show the temperature-dependent resistivity (ρ-T) curves for different n's. The ρ-T curves of the LPCMO alloy film and a 40-nm-thick LCMO film were also measured for comparison. Figures 2(b) and 2(c) show the deduced T_P and low-temperature resistivity ($\rho_{10\,K}$) values from the ρ-T cooling curves, respectively. For $n \leqslant 7$ superlattices, T_P decreases with increasing n and reaches a minimum value of 110 K, surprisingly close to that of the LPCMO alloy film (101 K). For $n > 7$, T_P increases with increasing n, exhibiting an n dependence similar to that of LCMO single-layer films (Fig. S6 [27]). For n large enough (e.g., $n = 18$), the superlattice behaves like LCMO films with similar T_P (240 K) and ρ-T curves. $\rho_{10\,K}$ exhibits a consistent n-dependent behavior, first

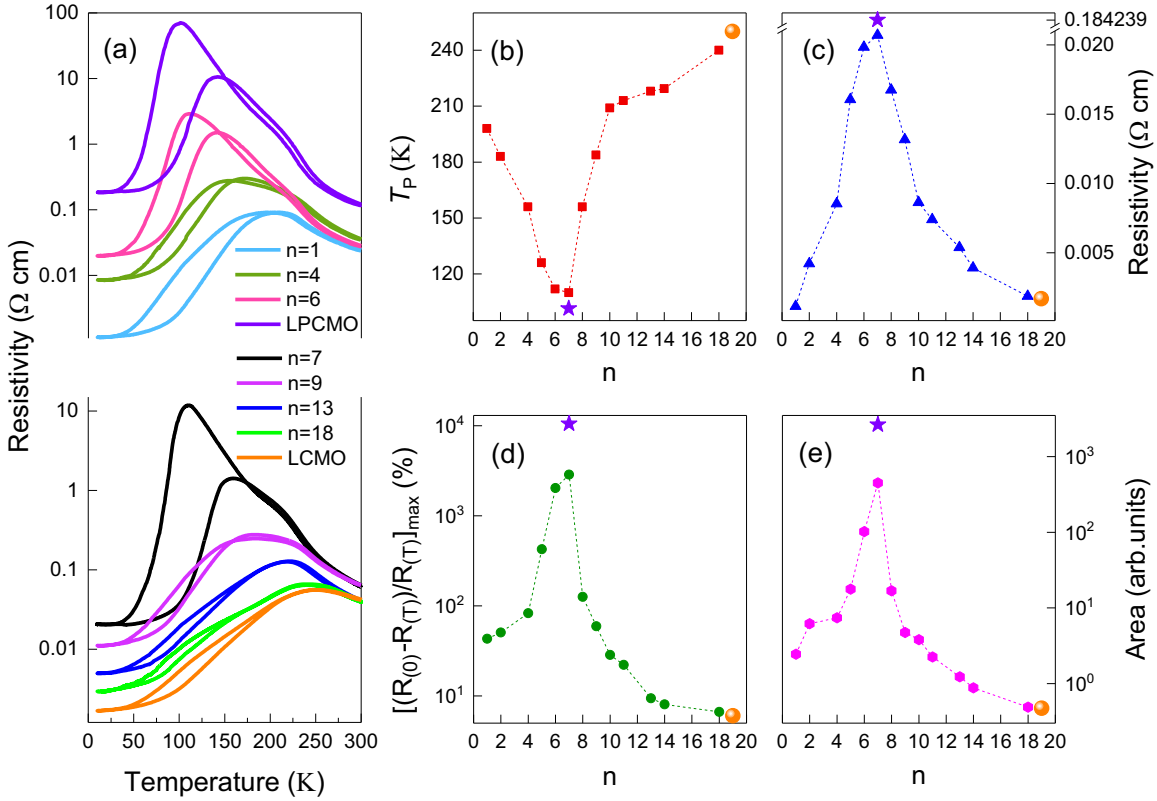

FIG. 2. Transport properties of the superlattice system. (a) Temperature-dependent resistivity (ρ-T) curves of n-dependent superlattices, LPCMO and LCMO films, measured at zero magnetic field. (b) n-dependent T_P (red square) from the cooling curve and (c) low-temperature resistivity (blue up triangle) measured at 10 K for all the superlattice samples. (d) Magnetoresistance (green circle) where MR $= (R_{(0)}–R_{(H)})/R_{(H)}$. (e) Integral area (magenta hexagon) of ρ-T curves between the cooling and warming curves, which reflects the thermal hysteresis. LCMO (orange spheres) and LPCMO (purple stars) are also marked in (b)–(e) for comparison.

increasing and then decreasing with increasing n. Remarkably, the maximum resistivity is reached *sharply* at $n = 7$. Figure 2(d) shows the maximum magnetoresistance (MR) obtained from the ρ-T curves. Here MR is defined as $(R_{(0)}–R_{(H)})/R_{(H)}$ with $R_{(0)}$ and $R_{(H)}$ representing resistivity measured at 0 and 9 T, respectively. Figure 2(e) shows the integral area of the thermal hysteresis between the cooling and warming ρ-T curves. The nonmonotonic turning points for both the n-dependent MR and thermal hysteretic area are reached at $n = 7$.

Figures 3(a) and 3(b) show temperature-dependent magnetization curves (M-T) and initial magnetization curves at 10 K after zero field cooling, respectively (details in Fig. S7 [27]). The M-T curves show two magnetic transitions, clearly identified by two distinct peaks of the slope of the $M(T)$ curve [see Fig. 3(c) inset for the $n = 1$ superlattice]. The high- and low-temperature peaks are known to represent the onset and percolation of FM domains, respectively [29]. We thus use the low-temperature peak to deduce T_C values [red arrows in inset of Fig. 3(c)]. The initial magnetization curves, at 10 K after zero field cooling, show a fast initial rise due to the magnetization of the existing FM phase, followed by a slow field-driven AFI to FM phase transition [30]. The FM phase volume fraction arises from the ratio between the initial fast rising magnetization and the saturation magnetization [inset Fig. 3(d)]. Figures 3(c) and 3(d) show the n dependence of the T_C and FM volume fraction reaching their minimum at $n = 6$ and $n = 7$, respectively. Interestingly, the minima for both T_C and the FM volume fraction are, once again, almost the same as those of the LPCMO alloy thin film. Beyond the minimum point, both the T_C and FM volume fraction increase with increasing n and exhibit a clear trend towards those of the 40-nm-thick LCMO thin film.

III. DISCUSSION

What causes the unexpected nonmonotonic dependence of the physical properties on the superlattice periodicity? Because of the LCMO-PCMO work function difference [31], charge transfer likely occurs at the LCMO/PCMO interface. This renders the interfacial PCMO layers more metallic, in turn enhancing the magnetic proximity effect and inducing ferromagnetism in the PCMO interfacial layers [12,32]. The vicinity of the LCMO/PCMO interfaces, thus, has a clear tendency towards ferromagnetism (Fig. S8 [27]). At the extreme $n = 1$, the superlattice consists only of LCMO/PCMO interfacial layers and has been observed to favor ferromagnetism with a considerably higher T_C and T_P than those of the LPCMO alloy [13]. Increasing n, the coupling between the FM interfacial layers weakens, as evidenced by the continuous reduction of T_C and T_P until $n = 6$–7 is reached.

Beyond the minimum points, both T_C and T_P start to increase with increasing n. The n dependence of T_P is nearly

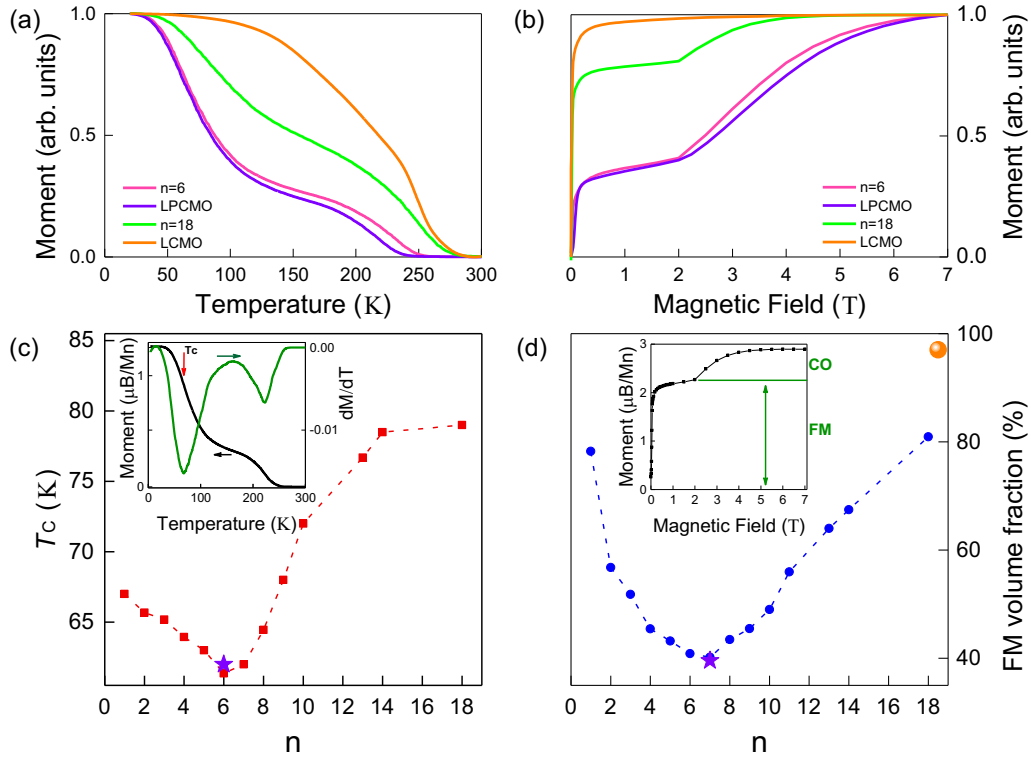

FIG. 3. Magnetic properties of the superlattice system. (a) Temperature-dependent magnetization curves (M-T). (b) Initial magnetization curves measured from 0 to 7 T after zero field cooling to 10 K. Both M-T curves and initial magnetization curves are normalized for better visualization. (c) n-dependent T_C of all the superlattice samples. Inset shows the temperature-dependent magnetization (M-T) of $n = 1$ SLs measured at 100 Oe, with T_C defined as the inflection points of $M(T)$ (indicated by arrows as shown in inset). (d) The FM volume fraction of each sample extracted from the initial magnetization curves measured at 10 K. The inset shows the initial magnetization curves of $n = 1$ SLs measured at 10 K after cooling from room temperature under zero magnetic field. T_C and FM volume fraction of LPCMO and LCMO films are also marked for comparison.

identical for the superlattices and the LCMO films (Fig. S6 [27]) clearly indicating that the $n > 7$ physical properties are dominated by the individual LCMO films, whose T_C and T_P increase with increasing thickness due to finite-size effects. The minima in T_C and T_P thus represent the crossover of two competing factors with opposite n dependence—the coupling strength between the LCMO/PCMO interfacial layers decays with increasing n while the intrinsic T_C and T_P of LCMO layers increase with n.

To support this point, we fabricated SLs with fixed thickness for the LCMO layers [8 UC (unit cells)] and varying PCMO layer thickness, i.e., $[(\mathrm{LCMO})_8/(\mathrm{PCMO})_x]_t$ superlattices ($x = 1,4,5,6,7,10$). The 8-UC LCMO thickness is chosen because the 8-UC LCMO film is a ferromagnetic insulator with $T_C \sim 98$ K, distinctly different from the behavior of the $[(\mathrm{LCMO})_{2n}/(\mathrm{PCMO})_n]_t$ superlattices and the LPCMO alloy thin films. Beyond the critical x, one would expect the LCMO/PCMO layers to decouple leading to a ferromagnetic insulating behavior with a distinctly lower T_C. Indeed, Fig. S9 in the Supplemental Material shows (a) the x dependence of FM volume fraction, (b) magnetic moment, (c) T_C, and (d) ρ-T curves [27]. Clearly, ferromagnetism and metallicity drop around $x = 6$, indicating that LCMO/PCMO interfacial layers are indeed decoupled when the PCMO layer thickness reaches 6 UC, in agreement with the n-dependent behavior of the $[(\mathrm{LCMO})_{2n}/(\mathrm{PCMO})_n]_t$ SLs. We thus conclude that the interface effect diminishes beyond 3 UC of PCMO layers (Fig. S10 [27]) [32].

The aforementioned competition between the interlayer coupling of LCMO/PCMO interfacial layers and the size of the LCMO layers is also reflected in the evolution of the EPS domain size with increasing n for the $[(\mathrm{LCMO})_{2n}/(\mathrm{PCMO})_n]_t$ superlattices. Figure 4(a) shows the n dependence of the EPS domain size measured by MFM, with the inset showing the corresponding MFM images for various n. The MFM images and domain size distribution were acquired at the same T/T_P (~1.05) for each n, right before the FM percolation. Figure 4(a) clearly shows that the FM phase domain size increases with increasing n and becomes comparable with that of the LPCMO alloy film for $n = 6$ or 7. For $n > 7$, the domain size decreases with increasing n, which is expected because the EPS domain size of the LCMO layers is known to be considerably smaller than that of the LPCMO system [33–35]. The n dependence of the EPS domain size distribution is summarized in Fig. S11 [27].

Here we discuss a simple calculation to understand qualitatively the relationship between the period n and the sizes of phase separated domains. We rely on the random-field Ising model (RFIM) for phase separation [13,36]. Physically, the competition between disorder and potential modulation tuned by the superlattice period determines the coexisting clusters. Typical simulation patterns for the surface layers are shown

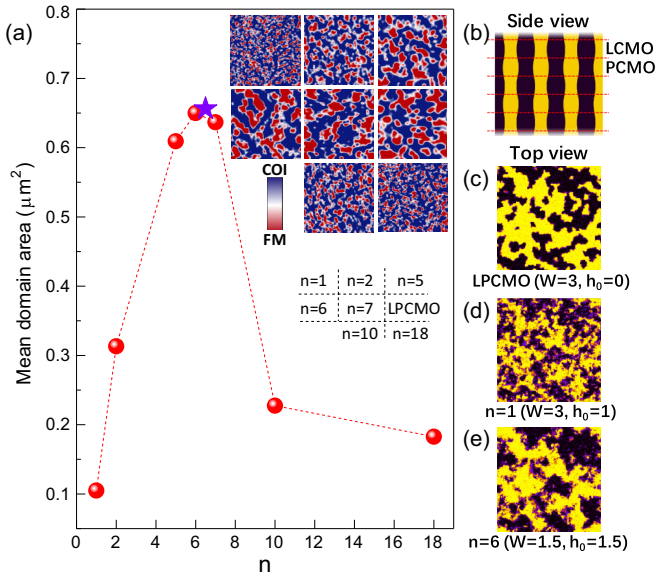

FIG. 4. MFM imaging and FMM domain size comparison. (a) Mean FM domain size of each $(LCMO)_{2n}/(PCMO)_n$ superlattices (red sphere) and LPCMO film (purple star). The domain size was analyzed from five images for each sample at each T/T_P temperature. Inset shows n-dependent MFM images (7 μm × 7 μm) at temperature T/T_P under 1 T field cooling (magnetic field applied perpendicular to sample surface). Areas with negative-phase signals are the FM states (red), while areas with zero-phase signal or positive-phase signals are charge-ordered insulating (COI) states (blue). (b) Schematic side view of phase separation. (c)–(e) Top view of the corresponding simulation of EPS for (c) bulk LPCMO, (d) $n = 1$ SLs, and (e) $n = 6$ SLs. Black: FM region; yellow: AFI region.

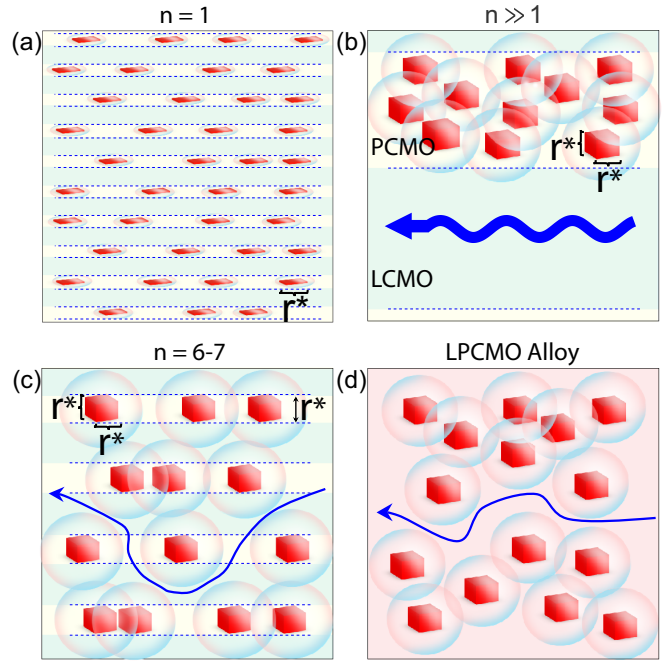

FIG. 5. Proposed explanation of our results. (a) At $n = 1$, random Pr clusters are flat, and not strong enough to seed large CO clusters. (b) At large n, the PCMO component (yellow) contains large Pr clusters inducing CO regions, but the LCMO component (green) dominates the metallic flow of charge. (c) At the critical $n^* = 6$–7, the size of randomly created Pr clusters that seed large CO clusters reaches the same optimal volume (crudely, a cube of size $r^* = n^*a$) that also seeds the charge-ordered (CO) clusters in the LPCMO alloy (pink), as shown in (d). In both (c,d) transport is percolative. The Pr clusters, CO clusters, and electric current are marked by red cubes, transparent bubbles, and blue arrows, respectively.

in Figs. 4(b)–4(e), qualitatively reproducing the experimental observation. Given the same volume ratio, the FM clusters become more fragmentary at small n, and the characteristic length scale of the AFI and FM phases is reduced compared to that of LPCMO; see Figs. 4(c) and 4(d). Increasing n, the modulation suppresses the EPS but the reduced randomness enhances the EPS (see "Model explanation" in the Methods section of the Supplemental Material [27]). This competition leads to the resulting characteristic length scale finally approaching typical sizes in LPCMO when $n = 6$, as shown in Fig. 4(e) (for details, see "Model simulation of EPS" in the Methods section [27]). According to our simulation, the more fragmentized the FM cluster is, the easier it is to reach the magnetic percolation, which may be helpful to understanding the physical tendency observed in our LCMO/PCMO superlattices and LPCMO thin films (for details, see Fig. S12 and "Model simulation of magnetic percolation" in the Methods section [27,37–39]).

Summarizing the experimental results, we presented the evolution of physical properties and EPS vs the $[(LCMO)_{2n}/(PCMO)_n]_t$ superlattice period. The ferromagnetism, metallicity, and length scale of EPS exhibit a nonmonotonic dependence on n, with the critical point at $n^* = 6$ or 7. Our experiments indicate the LCMO/PCMO interfacial layers have a strong tendency towards FM due to charge transfer. The nonmonotonic dependence originates from two competing factors with opposite trends: the coupling strength between the LCMO/PCMO interfacial layers decays with increasing n while the intrinsic T_C and T_P of the LCMO layers increases with n. As a result, the superlattices transit from a quasi-three-dimensional (3D)-like system of LCMO/PCMO interfacial layers at small n, to decoupled thick LCMO/PCMO layers at large n, was eventually dominated by the properties of the single LCMO regions at large n. This dimensionality crossover should be a general phenomenon for all superlattices with emerging interfacial properties.

This proposed general scenario allows us to formulate an explanation about the last piece of the puzzle, which is the remarkable resemblance in the physical characteristics of the n^* SLs with the LPCMO alloy, a percolated phase separated system. In previous theoretical studies [40] it was shown that chemical disorder plays a key role in nucleating regions of the competing metallic and insulating phases near a first-order phase transition. In alloy LPCMO, in the random distribution of atoms, small regions rich in Pr of the proper size, dubbed r^*, are formed. These regions can nucleate much larger charge-ordered clusters; i.e., we remark that these Pr-rich regions are certainly *not* submicrometer in size, but of the scale of a few lattice spacings. In the abnormally fragile regime of competition metal versus insulator in LPCMO even small amounts of seeding disorder have vastly amplified consequences, as shown theoretically in Ref. [40] when two states

are in close competition through a first-order transition. In our SLs, at large n the LCMO metallic regions shortcut the large insulating PCMO components [Fig. 5(b)] and charge only conducts through LCMO. That is, at large n, the size of Pr aggregates is irrelevant for global transport. At small n, Pr can only randomly accumulate in individual planes forming "Pr-rich pancakes" but not form the required 3D-like seeding region of diameter r^* [Fig. 5(a)]. However, clearly there must be an intermediate n^* value where the random distribution of Pr in PCMO can reach the size of r^* in the LPCMO alloy, i.e., $r^* = n^* a$ with "a" being the lattice spacing perpendicular to the interfaces, leading to the submicrometer phase-separation properties similar to LPCMO [Figs. 5(c) and 5(d)]. Thus, we have indirectly found that in the LPCMO alloy the critical disorder seed size is $r^* = 6$–$7a$. Our study has general implications. In [34] a widely discussed scenario to explain the abnormally large coexisting clusters in LPCMO was formulated: Disorder can nucleate abnormally large regions of two different competing phases near a first-order transition, but in that coarse-grain phenomenological calculation employing the random-field Ising model, with spin up denoting one phase and spin down the other phase, [34] disorder was on site and uncorrelated from site to site. Here we conjecture that a critical length scale r^* for disorder appears to be needed for the generation of LPCMO's giant cluster coexistence. This conjecture is generic and should affect any first-order transition that is smeared by quenched disorder into large cluster coexistence.

ACKNOWLEDGMENTS

The authors are especially thankful to Xiaoguang Zhang for valuable discussions. We thank beamline BL14B1 (Shanghai Synchrotron Radiation Facility) for providing the beam time and help during experiments. This work was supported by the National Key Research and Development Program of China (2016YFA0300702), National Natural Science Foundation of China (Grants No. 11904052, No. 11991060, No. 12074075, No. 12074073, and No. 12074071), the Program of Shanghai Academic Research Leader (18XD1400600), and the Shanghai Municipal Natural Science Foundation (Grants No. 18JC1411400, No. 18ZR1403200, No. 19ZR1402800, and No. 20501130600). E.D. was supported by the U.S. Department of Energy (DOE), Office of Science, Basic Energy Sciences (BES), Materials Science and Engineering Division.

[1] M. Nakamura, D. Okuyama, J. S. Lee, T. Arima, Y. Wakabayashi, R. Kumai, M. Kawasaki, and Y. Tokura, Adv. Mater. **22**, 500 (2010).

[2] K. Rogdakis, J. W. Seo, Z. Viskadourakis, Y. Wang, L. Qune, E. Choi, J. D. Burton, E. Y. Tsymbal, J. Lee, and C. Panagopoulos, Nat. Commun. **3**, 1064 (2012).

[3] X. F. Zhai, L. Cheng, Y. Liu, C. M. Schlepuetz, S. Dong, H. Li, X. Q. Zhang, S. Q. Chu, L. R. Zheng, J. Zhang, A. D. Zhao, H. Hong, A. Bhattacharya, J. N. Eckstein, and C. G. Zeng, Nat. Commun. **5**, 4283 (2014).

[4] T. Koida, M. Lippmaa, T. Fukumura, K. Itaka, Y. Matsumoto, M. Kawasaki, and H. Koinuma, Phys. Rev. B **66**, 144418 (2002).

[5] D. Yi, C. L. Flint, P. P. Balakrishnan, K. Mahalingam, B. Urwin, A. Vailionis, A. T. N'Diaye, P. Shafer, E. Arenholz, Y. Choi, K. H. Stone, J.-H. Chu, B. M. Howe, J. Liu, I. R. Fisher, and Y. Suzuki, Phys. Rev. Lett. **119**, 077201 (2017).

[6] Z. Zanolli, J. C. Wojdel, J. Iniguez, and P. Ghosez, Phys. Rev. B **88**, 060102(R) (2013).

[7] S. J. May, P. J. Ryan, J. L. Robertson, J. W. Kim, T. S. Santos, E. Karapetrova, J. L. Zarestky, X. Zhai, S. G. E. te Velthuis, J. N. Eckstein, S. D. Bader, and A. Bhattacharya, Nat. Mater. **8**, 892 (2009).

[8] T. Miao, L. N. Deng, W. T. Yang, J. Y. Ni, C. L. Zheng, J. Etheridge, S. S. Wang, H. Liu, H. X. Lin, Y. Yu, Q. Shi, P. Cai, Y. Y. Zhu, T. Y. Yang, X. M. Zhang, X. Y. Gao, C. Y. Xi, M. L. Tian, X. S. Wu, H. J. Xiang *et al.*, Proc. Natl. Acad. Sci. USA **117**, 7090 (2020).

[9] D. Yi, J. Liu, S. L. Hsu, L. P. Zhang, Y. Choi, J. W. Kim, Z. H. Chen, J. D. Clarkson, C. R. Serrao, E. Arenholz, P. J. Ryan, H. X. Xu, R. J. Birgeneau, and R. Ramesh, Proc. Natl. Acad. Sci. USA **113**, 6397 (2016).

[10] M. Gibert, P. Zubko, R. Scherwitzl, J. Iniguez, and J. M. Triscone, Nat. Mater. **11**, 195 (2012).

[11] M. Ziese, I. Vrejoiu, E. Pippel, P. Esquinazi, D. Hesse, C. Etz, J. Henk, A. Ernst, I. V. Maznichenko, W. Hergert, and I. Mertig, Phys. Rev. Lett. **104**, 167203 (2010).

[12] Y. Yamasaki, D. Okuyama, M. Nakamura, T. Arima, M. Kawasaki, Y. Tokura, T. Kimura, and Y. Wakabayashi, J. Phys. Soc. Jpn. **80**, 073601 (2011).

[13] Y. Y. Zhu, K. Du, J. B. Niu, L. F. Lin, W. G. Wei, H. Liu, H. X. Lin, K. Zhang, T. Y. Yang, Y. F. Kou, J. Shao, X. Y. Gao, X. S. Xu, X. S. Wu, S. Dong, L. F. Yin, and J. Shen, Nat. Commun. **7**, 11260 (2016).

[14] Ariando, X. Wang, G. Baskaran, Z. Q. Liu, J. Huijben, J. B. Yi, A. Annadi, A. R. Barman, A. Rusydi, S. Dhar, Y. P. Feng, J. Ding, H. Hilgenkamp, and T. Venkatesan, Nat. Commun. **2**, 188 (2011).

[15] Y. Wang, Y. Zhu, H. Liu, H. Lin, T. Miao, Y. Yu, F. Han, W. Wang, J. Sun, L. Yin, and J. Shen, J. Mater. Chem. C **6**, 1224 (2018).

[16] E. Dagotto, Science **309**, 257 (2005).

[17] E. Dagotto, New J. Phys. **7**, 67 (2005).

[18] J. Shen, T. Z. Ward, and L. F. Yin, Chin. Phys. B **22**, 017501 (2013).

[19] P. Schiffer, A. P. Ramirez, W. Bao, and S. W. Cheong, Phys. Rev. Lett. **75**, 3336 (1995).

[20] E. Dagotto, T. Hotta, and A. Moreo, Phys. Rep. **344**, 1 (2001).

[21] Y. Tomioka, A. Asamitsu, H. Kuwahara, Y. Moritomo, and Y. Tokura, Phys. Rev. B **53**, R1689 (1996).

[22] Y. Tokura and Y. Tomioka, J. Magn. Magn. Mater. **200**, 1 (1999).

[23] M. Uehara, S. Mori, C. H. Chen, and S. W. Cheong, Nature **399**, 560 (1999).

[24] L. W. Zhang, C. Israel, A. Biswas, R. L. Greene, and A. de Lozanne, Science **298**, 805 (2002).
[25] H. Lin, T. Miao, Q. Shi, Y. Yu, H. Liu, K. Zhang, W. Wang, L. Yin, and J. Shen, Sci. China: Phys., Mech. Astron **61**, 97511 (2018).
[26] Y. Yu, Q. Li, Q. Shi, Y. Y. Zhu, H. X. Lin, H. Liu, H. Y. Chen, T. Miao, Y. Bai, Y. M. Wang, W. T. Yang, W. B. Wang, H. W. Guo, L. F. Yin, and J. Shen, Sci. China: Phys., Mech. Astron. **63**, 237811 (2020).
[27] See Supplemental Material at http://link.aps.org/supplemental/10.1103/PhysRevB.102.235107 for extra RHEED intensity oscillation, x-ray diffraction data, EELS spectrum image, transport and magnetic data, and experimental methods.
[28] T. Y. Yang, W. Wen, G. Z. Yin, X. L. Li, M. Gao, Y. L. Gu, L. Li, Y. Liu, H. Lin, X. M. Zhang, B. Zhao, T. K. Liu, Y. G. Yang, Z. Li, X. T. Zhou, and X. Y. Gao, Nucl. Sci. Tech. **26**, 020101 (2015).
[29] M. Uehara and S. W. Cheong, Europhys. Lett. **52**, 674 (2000).
[30] J. X. Ma, D. T. Gillaspie, E. W. Plummer, and J. Shen, Phys. Rev. Lett. **95**, 237210 (2005).
[31] D. W. Reagor, S. Y. Lee, Y. Li, and Q. X. Jia, J. Appl. Phys. **95**, 7971 (2004).
[32] A. Ohtomo, D. A. Muller, J. L. Grazul, and H. Y. Hwang, Nature **419**, 378 (2002).
[33] J. Tao, D. Niebieskikwiat, M. Varela, W. Luo, M. A. Schofield, Y. Zhu, M. B. Salamon, J. M. Zuo, S. T. Pantelides, and S. J. Pennycook, Phys. Rev. Lett. **103**, 097202 (2009).
[34] M. Bibes, L. Balcells, S. Valencia, J. Fontcuberta, M. Wojcik, E. Jedryka, and S. Nadolski, Phys. Rev. Lett. **87**, 067210 (2001).
[35] E. Dagotto, *Nanoscale Phase Separation and Colossal Magnetoresistance*, Berlin ed. (Springer, Berlin, 2003).
[36] A. Moreo, M. Mayr, A. Feiguin, S. Yunoki, and E. Dagotto, Phys. Rev. Lett. **84**, 5568 (2000).
[37] S. Dong, H. Zhu, and J. M. Liu, Phys. Rev. B **76**, 132409 (2007).
[38] S. Dong, H. Zhu, X. Wu, and J. M. Liu, Appl. Phys. Lett. **86**, 022501 (2005).
[39] H. W. Guo, J. H. Noh, S. Dong, P. D. Rack, Z. Gai, X. S. Xu, E. Dagotto, J. Shen, and T. Z. Ward, Nano Lett. **13**, 3749 (2013).
[40] J. Burgy, M. Mayr, V. Martin-Mayor, A. Moreo, and E. Dagotto, Phys. Rev. Lett. **87**, 277202 (2001).